

5

Large eddy simulations of cloud-topped mixed layers

Chin-Hoh Moeng¹, Bjorn Stevens² and Peter P. Sullivan¹

¹ National Center for Atmospheric Research, Boulder, CO 80523

² Department of Atmospheric and Oceanic Sciences, University of
California, Los Angeles, CA 90095-1565

5.1 Introduction

With the advent of computers, scientists in the 1950s and 1960s began to explore the possibility of using numerical simulation to generate virtual laboratories for exploring specific geophysical processes in a controlled manner. Doug Lilly helped pioneer this emerging science of numerical simulation. As pointed out by Wyngaard (Chpt 1), Lilly presented a “bold, three phase plan of attack” in which well-behaved numerical models would be developed; their fidelity would be benchmarked against known solutions; and as confidence builds they would be used to explore conditions not adequately reproducible by experiment. In the subsequent decades this strategy has become a staple of theoretical studies of turbulence. In particular, a class of numerical simulations Doug helped develop in the early 1960s has come to be known as large-eddy simulation (LES) and is now widely used in the field of atmospheric boundary layer (PBL) turbulence and clouds.

We begin in section 5.2 by giving an example of the second element of Doug’s plan of attack, and what we call “benchmarking.” This is by no means trivial because for turbulent flows, there are no known solutions. To better appreciate this point we consider LES of the cloud-topped boundary layer which couples turbulence, radiation, and cloud processes. As cloudy boundary layers cannot be created in the laboratory, one must invariably turn to field data to construct meaningful benchmarks. Historically, field data have been collected to explore phenomenology, and thus few datasets exist to benchmark computations. The second field study of the Dynamics

and Chemistry of Marine Stratocumulus (DYCOMS-II) is unique in that it was designed from the outset with the purpose of testing LES. However, even with this focused field campaign the measurements needed to design an LES to completely mimic the natural environment are difficult to make, and as we shall see this element of Doug’s strategy remains in its infancy.

The third element of Doug’s strategy emphasizes creative thinking. Simulations can be used to explore the parameter space that has not been (or cannot be) measured in the field; or, for a given set of parameters, simulations can be used to explore physical aspects of the solution that cannot be measured. Both tactics require theoretical guidelines. In the former one needs a theoretical framework to help guide exploration of the parameter space and in the latter (which we focus on here) a theoretical framework is needed to pose stimulating questions. A proper theoretical framework for the stratocumulus-topped boundary layer is Lilly’s mixed layer theory (see the review by Randall and Schubert, chapter 4). With this theoretical framework and some early LES solutions, Lilly investigates how the structure of the cloud-top interface may affect its statistical representation (Lilly 2002a), and how the interface property can change the entrainment rate and interface stability (Lilly 2002b). As we show in sections 5.3 and 5.4 both questions are impossible to attack with observations alone, but fit the third phase of Doug’s “bold plan of attack” on geophysical turbulence problems.

5.2 Benchmarking

For the purpose of benchmarking LES we use data collected as part of DYCOMS-II. An overview of the experiment is given in Stevens *et al.*, (2003a); the particular case we focus on here, research flight one (RF01), is an outgrowth of an earlier study of the case described by Stevens *et al.*, (2003b). The appealing aspect of DYCOMS-II is that it is predominantly nocturnal, which makes it relatively straightforward to constrain the large-scale energetics. An appealing aspect of RF01 is that the stratocumulus layer is essentially non precipitating, and the large-scale conditions are remarkably uniform, further simplifying possible comparisons with LES. The code used throughout is the NCAR LES, which was described in Moeng (1986) and more recently in Moeng (2000).

H_0	15 Wm^{-2}
L_0	100 Wm^{-2}
D	$4 \times 10^{-6} \text{ s}^{-1}$
(U_g, V_g)	$(6, -4.25) \text{ ms}^{-1}$
z_0	0.00002 m
f	$1 \times 10^{-4} \text{ s}^{-1}$
p_0	0.1 MPa
Θ_0	288 K

Table 5.1. *Input parameters, where H_0 and L_0 denote the surface sensible and latent heat fluxes respectively, D the large-scale divergence, U_g and V_g the geostrophic wind, z_0 the roughness height, f the Coriolis frequency, p_0 the surface pressure, and Θ_0 the reference temperature.*

5.2.1 Set-up and initial data

The initial data and boundary forcings for the LES were derived from the RF01 measurements as reported by Stevens *et al.*, (2003b). This case is characterized as a persistent, well-mixed, and slightly thickening nocturnal cloud field capped by a much warmer and drier free-troposphere. The large-scale conditions were approximately constant over the measurement period (which spanned 8 hours). Input parameters for the LES are given in Table 5.1. For the vertically varying basic state we specify

$$\{q_T, \theta_l\} = \begin{cases} \{8.75 \text{ g kg}^{-1}, 289.7 \text{ K}\} & z < 817\text{m}, \\ \{1.50 \text{ g kg}^{-1}, [296.7 + (z - 817)^{1/3}] \text{ K}\} & \text{otherwise,} \end{cases} \quad (5.1)$$

where θ_l is the liquid water potential temperature and q_T is the total water mixing ratio. In addition to the surface fluxes, radiative forcing also drives the flow; here it is calculated from a simple exponential formula, which using Lilly's (2002b) notation is expressed as follows:

$$F_R = F_i \exp\left(\frac{z - z_i}{\lambda}\right), \quad \text{for } z \leq z_i, \quad (5.2)$$

where z_i is the local cloud top, $F_i = 50 \text{ Wm}^{-2}$ is the net radiative flux above cloud top derived from measurements. The decay length scale $\lambda \approx 1/(\rho_0 \kappa q_l) \approx 26\text{m}$ given a reference air density of 1 kg m^{-3} , a long-wave absorption coefficient $\kappa = 130 \text{ m}^2\text{kg}^{-1}$ and an assumed mean cloud-top liquid water mixing ratio of 0.3 g kg^{-1} . Note that these parameters and initial data differ somewhat from the observations and from our previous investigation of this case (i.e., Stevens *et al.* 2003b). Here changes have been

made to preserve the cloud layer through the initial spin-up period of the simulation, and to compensate for the use of an assumed Boussinesq vertical structure with $\rho_0 = 1 \text{ g kg}^{-1}$.

Below we explore results from three simulations, LES-(1,2,3), which differ only in their numerical treatment. Cases LES-(1,2) both span a domain of $2500 \text{ m} \times 2500 \text{ m} \times 1500 \text{ m}$ with a mesh of $96 \times 96 \times 400$ points, and only differ in their treatment of the horizontal advection terms in the θ_l and q_T equations; LES-1 uses a pseudo-spectral method, while LES-2 uses the flux-limited upwind algorithm (Koren 1993, Sullivan *et al.*, 1998) that is employed for the vertical advection in all 3 simulations. LES-3 is identical to LES-1 except that it spans a $7500 \text{ m} \times 7500 \text{ m} \times 1500 \text{ m}$ domain with a mesh of $200 \times 200 \times 400$ points. The increased size of the horizontal domain is computationally expensive, so LES-3 is integrated for only two simulation hours, as compared to four simulation hours for LES-(1,2). Thus in the spirit of benchmarking, we ask not only if the LES can reproduce the observed structure with plausible fidelity, but also if this reproduction is sensitive (at short times) to numerical methods or the truncation of larger scales.

5.2.2 Comparison between LESs and observations

We compare the simulations only after the first hour. Before this time, the turbulence is not fully developed and the statistics are not stationary. Stationarity of the statistics is associated with invariance in the shapes of the profile statistics. Specifically, for a conserved variable, ψ , whose horizontal average, Ψ , satisfies

$$\partial_t \Psi = \partial_z \Phi, \quad (5.3)$$

where Φ is some flux, then this condition implies that $\partial_t \partial_z \Psi$ vanishes, or equivalently Φ is linear. If this condition is satisfied, the turbulent flow is near statistical equilibrium. LES is most justifiably used to study the statistical properties of turbulent flow fields; for this reason its analysis is normally confined to time periods when the turbulence is in statistical equilibrium or the so-called quasi-steady state.

In Fig. 5.1 we show how the simulations represent the cloud evolution, and the numerical effects on this evolution. The fractional cloud cover stays at about 99.5% in LES-1 and fluctuates between 85% to 92% in LES-2. The time evolution of the cloud top and base given in Fig. 5.1 are quite similar

¹ For instance the turbulent flux $\overline{wq_T}$ in the case that $\Psi = Q_T$, or the combination of the turbulent heat flux and the radiative flux when $\Psi = \Theta_l$.

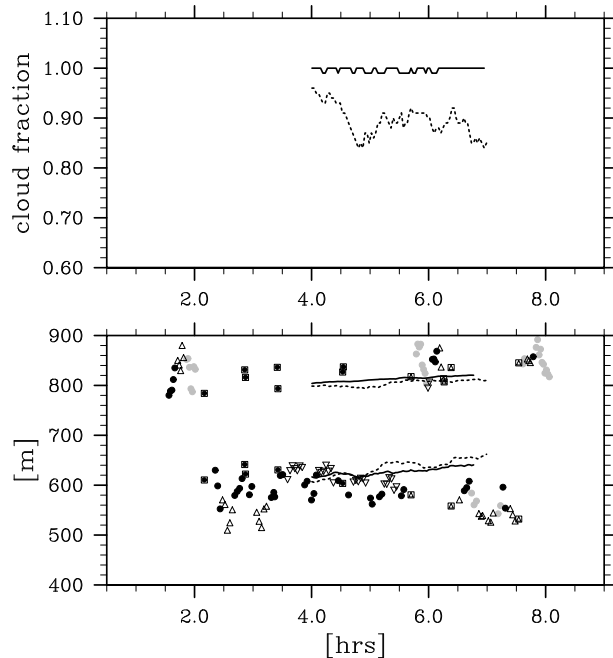


Figure 5.1. Time evolution of the fractional cloud cover (upper panel) and the mean cloud-top and cloud-base heights (lower panel) from LES-1 (solid lines), LES-2 (dotted lines), and observations adapted from Stevens *et al.*, 2003b. Here the starting time of the simulation relative to the time of observation is chosen to roughly correspond to the initial data of the simulations. Note that the mean cloud top and base heights are computed by horizontally averaging the local cloud tops and bases only over cloudy grid points.

between LES-1 and LES-2 although LES-2 grows thinner compared to LES-1. Overall, the LESs compare well with the observations, although there is a tendency for cloud base to rise through the course of the simulation, in contrast to its apparent lowering in the field data. As we shall see this is consistent with a simulated entrainment moisture flux that is larger than the observed. The simulations show that the mean cloud top rises at a rate of about 0.16 cm s^{-1} , and hence given a large-scale subsidence of $\sim 0.32 \text{ cm s}^{-1}$ at $z = 810 \text{ m}$, this rate of PBL deepening implies an entrainment rate of about 0.48 cm s^{-1} , which is in the range of observed values (Stevens *et al.*, 2003b).

The profile statistics from LES are computed as follows. We first compute statistics by applying horizontal ($x - y$) averaging, then interpolate these instantaneous profile statistics to a normalized vertical coordinate z/\bar{z}_i (where \bar{z}_i is the horizontally averaged cloud-top height), and finally time-average

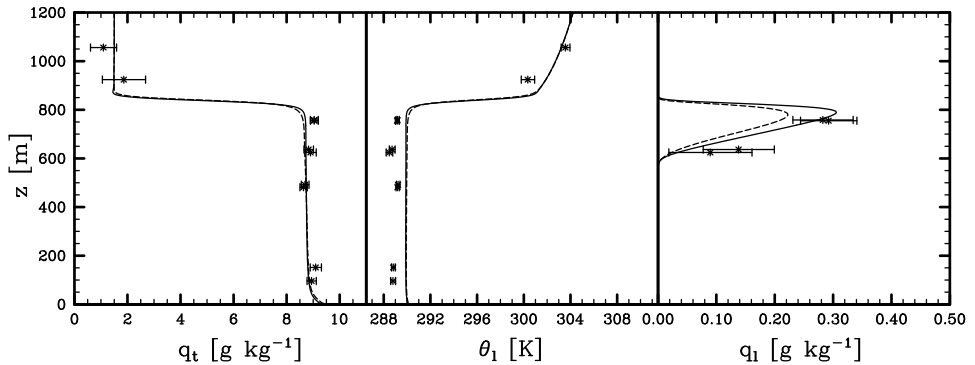


Figure 5.2. Vertical profiles of (a) total water mixing ratio, (b) liquid water potential temperature, and (c) liquid water mixing ratio from LES-1 (solid curves), LES-2 (dotted curves), and the observations adapted from Stevens *et al.*, 2003b

these profiles between hour 1 and 4 of the simulation period. Because the vertical normalization is based on the spatially averaged cloud-top height, the transition across the cloud top is expected to be smoothed across a scale corresponding to spatial fluctuations in the simulated interfacial layer at any given time. In the third part of this chapter we investigate the effect of this smoothing. Figure 5.2 shows vertical profiles of Q_T , Θ_l , and Q_l for LES-(1,2) compared with the observed sounding taken from Stevens *et al.* (2003b). These results show that the LES provides a plausible representation of the cloud-topped mixed layer and the simulations maintain a jump structure similar to what was observed. No decoupling occurs; the PBL remains well mixed throughout the simulations.

The comparison of the mean states can be more critically evaluated by comparing the time-rate-of-change of θ_l and q_T within the mixed layer. Such comparisons (not shown here) indicate that the simulated layer is warming more rapidly (about 0.1 K h^{-1} versus the observed rate of 0.07 K h^{-1}), and not moistening as quickly ($0.02 \text{ g kg}^{-1} \text{ h}^{-1}$ versus the observed rate of $0.06 \text{ g kg}^{-1} \text{ h}^{-1}$). These differences are not large, but both contribute to the simulation tendency to raise cloud base. Such differences are consistent with simulated entrainment rates being on the upper end of the observed range.

Figures 5.3 and 5.4 show the effective enthalpy flux, as well as fluxes of moisture and buoyancy from LES-1 and LES-2. The thick solid curves denote total (resolved plus subfilter) fluxes. The total flux of moist enthalpy ($H \equiv \rho c_p \overline{w\theta_l} + F_R$) and the total moisture flux are linear with height as required by our condition of quasi-steady state. The effect of using an upwind

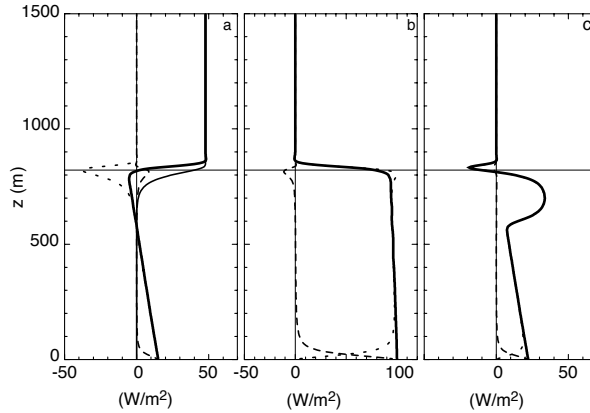


Figure 5.3. Vertical profiles of (a) heat fluxes (dotted curve is the resolved-scale θ_l -flux, thin solid curve the longwave radiative flux, dashed curve the SFS θ_l -flux, thick solid curve the total heat flux H); (b) moisture fluxes (dotted curve is the resolved-scale q_T -flux, dashed curve the SFS q_T -flux, and thick solid curve the total); (c) buoyancy fluxes (dotted curve is the resolved-scale θ_v -flux, dashed curve the SFS θ_v -flux, and thick solid curve the total) from LES-1. The thin horizontal line represents the minimum θ_l -flux level.

scheme on the horizontal advection of scalars is evident in the individual components of the resolved and subfilter-scale (SFS) fluxes near the cloud top where the temperature and moisture gradients are large. In LES-1, the SFS heat flux is positive and the SFS moisture flux is negative, while in LES-2 these SFS fluxes reverse signs. This highlights the difficulty of treating SFS terms, which operate most effectively at the grid-scale where numerical errors are most evident. Here we simply note that in LES-1 the truncation error (due to overshoots) over-estimates the resolved-scale moisture flux near cloud top and is combatted by the SFS model to maintain a linear profile of the total flux.

The difference in H above the cloud layer between LES-1 and LES-2 reflects a smaller radiative flux due to a smaller fractional cloud cover in LES-2 than in LES-1. This smaller radiative forcing also results in a smaller buoyancy flux in the cloud layer of LES-2.

The mean moisture and moisture flux profiles shown above can be used to estimate the entrainment rate because $\overline{wq_T} \equiv -w_e \Delta Q_T$ for non-precipitating cloud. From Fig. 5.2a, we estimate a moisture jump of about -7.25 g kg^{-1} . Both Figs. 5.3b and 5.4b show that the entrainment moisture

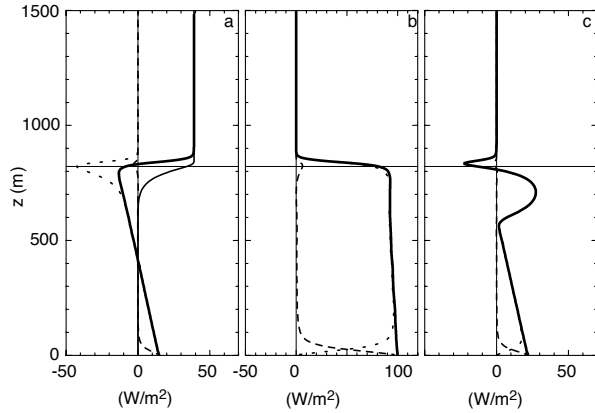


Figure 5.4. Same as Fig. 5.3 except for LES-2.

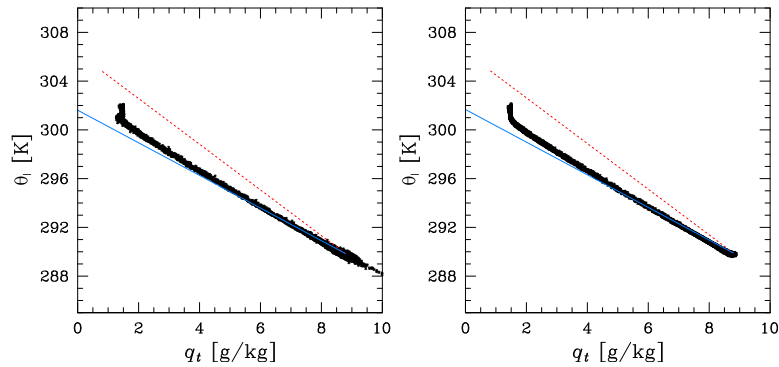


Figure 5.5. Plot of θ_l and q_T from the LES grid points between 750 m and 900 m. The blue line is taken from figure 6 of Stevens *et al.* (2003b) and the red line represents the the Deardorff-Randall CTEI criterion. Left panel: LES-1; Right panel: LES-2

flux is about 90 Wm^{-1} , which is somewhat larger than the observed (see Fig. 8a in Stevens *et al.* 2003b). This simulated moisture flux yields an entrainment rate of about 0.50 cm s^{-1} , consistent with the estimate from the time change of the mean cloud-top height given above. Given that the entrainment rates are similar in LES-1 and LES-2, the larger radiative driving for LES-1 (implicit in the larger above-cloud values of H and a smaller layer averaged buoyancy fluxes) suggests that entrainment is somewhat more efficient in LES-2.

Our motivation for using the flux-limited upwind (i.e., monotone) scheme for horizontal advection in LES-2 is evident in the mixing line plot of the LES-1 solution, shown in the left panel of Fig. 5.5. The dots are LES solutions from the layer between $z = 750$ m and 900 m (i.e., near the cloud-top regions) at hour 2. The blue line represents the observed mixing line (from Stevens *et al.*, 2003b) and the red line indicates the Deardorff-Randall cloud-top entrainment instability (CTEI) criterion (from Deardorff 1980; Randall 1980). The intersection between the red and blue lines is calculated by layer-averaging the LES θ_l and q_T fields below $z = 700$ m, and is representative of the bulk mixed-layer properties, $\Theta_{l_{\text{mix}}} \sim 290$ K and $Q_{T_{\text{mix}}} \sim 8.75$ g kg⁻¹. In the LES-1 case, at the upper end of the mixing line, global minima develop (i.e., points with $q_T < 1.5$ g kg⁻¹). At the lower terminus some global maxima are evident (i.e., points with $q_T > 9$ g kg⁻¹). Neither can be justified on physical grounds. They are numerical artifacts which arise because the cloud top undulates in the presence of a mean wind so that horizontal advection also advects θ_l and q_T across sharp interfaces. The pseudo-spectral scheme used for the horizontal advection of scalars in LES-1 results in truncation errors consistent with these extrema. We therefore implemented a flux-limited upwind scheme, which is used for vertical advection of scalars, for horizontal advection of scalars in LES-2. The extrema at both ends of the mixing line disappears in LES-2, as shown in the right panel of Fig. 5.5. Although the upwind scheme in LES-2 eliminates the spurious extrema, the bulk property of the mixing line is relatively unchanged between LES-1 and LES-2.

Because there are no spurious data points at the ends of the mixing line in LES-2, we use the right panel of Fig. 5.5 to estimate jumps in Θ_l and Q_T . The jumps of Θ_l and Q_T are computed as the differences between the end points of the mixing line (before the curve turns at the upper end), and that leads to $\Delta\Theta_l \sim 11$ K and $\Delta Q_T \sim -7.2$ g kg⁻¹ at hour 2 of the simulation. Using these jumps, we obtain the Randall-Deardorff CTEI parameter $\kappa \equiv \Delta\Theta_e / (L/c_p)\Delta Q_T \sim 0.38$, where $\kappa > 0.23$ is hypothesized for breakup of cloud by Randall (1980) and Deardorff (1980). (Here $\Theta_e \sim \Theta_l + (L/c_p)Q_T$ is the equivalent potential temperature.) At the end of the simulation $\Delta\Theta_l$ grew to about 11.5 K, which results in a slightly steeper mixing line (not shown) than that shown in Fig. 5.5; nevertheless, throughout the four hours of simulation the mixing lines remain on the “unstable” side of the Randall-Deardorff criterion (i.e., $\kappa > 0.23$), as did the observed cloud, but the cloud layer remains solid.

5.2.3 Large-scale truncation

The time series of the liquid water field from DYCOMS-II in-cloud flight legs (Faloona, personal communication) often show fluctuations on scales larger than the domain size of LES-1 and LES-2. This raises the question as to whether the truncation of scales larger than the numerical domain biases the resultant statistics. To investigate this issue we conducted LES-3, whose domain was a factor of three larger. For the most part the statistics were insensitive to the presence of larger scales (although truly large-scale variations may not have had time to spin-up in this short time period). The cloud field in LES-3 reveals the presence of scales larger than 2.5 km, which compares more favorably with observations, but these larger-scale fluctuations do not change the statistics examined here.

5.3 Sharp-edged framework

Having demonstrated that LES plausibly represents a real flow, we now use it to address specific scientific questions. The first (e.g., Lilly 2002a) arises in response to lingering criticisms of mixed-layer theory which, as originally formulated (Lilly 1968), rests on the idealization of the cloud-top interface as a discontinuity in the mean thermodynamic profiles. This so-called zero-order jump condition (see chapter by Randall and Schubert) has been criticized in part because field measurements and LES (e.g., Betts 1974, Deardorff 1979) often show a smooth transition in state variables over a non-negligible depth across the top of the mixed layer. To address this criticism, Lilly (2002a,b) introduced an interface tracking coordinate which he identified with the local position of the entrainment interface. His idea was that the apparent diffusiveness in averaged entrainment interfaces could be a product of averaging over a locally sharp top that fluctuates in space and time. By working in a coordinate system following the local interface, Lilly argues that such artifacts can be avoided.

5.3.1 Cloud-top interface

Central to Lilly's argument is the idea that the cloud top constitutes an unambiguous interface. However in practice, nothing is unambiguous. For example in Fig. 5.6, we plot the location of two interfaces: (1) the liquid-water interface defined as the uppermost level where the liquid water field changes from non-zero to zero, which is shown as a solid curve and denoted as z_{lwc} , and (2) the maximum- θ_l -gradient interface defined as the height

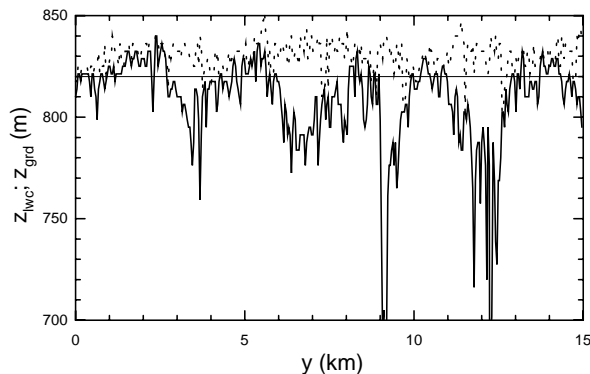


Figure 5.6. Spatial variation of the liquid-water interface (solid curve) and the maximum- θ_l -gradient interface (dotted curve) from LES-3. The horizontal line is the mid-level of the liquid-water interface undulation, which contains approximately equal amounts of clear and cloudy air.

where the maximum vertical gradient of θ_l occurs, which is shown as a dotted curve and denoted as z_{grd} . (We also checked the maximum- q_T -gradient interface, and found it is nearly coincident with the z_{grd} interface.) To see the fluctuations in a larger domain, we combine two different horizontal segments of the LES-3 solution (each 7.5 km long) to form a total domain of 15 km.

These two interfaces do not coincide: z_{grd} is most often above z_{lwc} , and the gap between them becomes wider where z_{lwc} is smaller; this is similar to what was observed by Stevens *et al.*(1999) for the case of a smoke cloud. Here we see that the vertical separation can be more than 100 m. These cloud-top fluctuations reveal some interesting physical processes near the cloud top. The interface (particularly when identified with z_{lwc}) is higher than average above vigorous updrafts. As these updrafts penetrate into the inversion, they squeeze the constant θ_l surfaces aloft intensifying the maximum gradient right above them. Thus, in these segments z_{grd} is likely to be about the same as z_{lwc} , both near the top of the penetrating updrafts. Adjacent regions tend to have greater separation between z_{grd} and z_{lwc} in part for kinematic reasons. Similar effects are evident in the study of the dry convective boundary layer, *cf.*, Sullivan *et al.*(1998), and the smoke-cloud, *cf.*, Stevens *et al.*(1999). However in contrast to both the smoke cloud and the dry CBL, in the stratocumulus topped PBL the manner in which the top of the layer is affected by mixing depends on how the top of the layer is defined — in large part because cloud top is not a material surface. If some inversion air is entrained and mixed in with these returning eddies, mixtures

of clear and cloudy air can be expected to characterize the properties of the air near cloud top. Mixtures with small amounts of inversion air remain saturated, while those with more inversion air totally evaporate and become non-cloudy air. Similarly, in regions of active mixing the θ_l gradients will be reduced and thus the level where the gradient attains its maximum value can be expected to be above these active mixing regions. Hence, this process can simultaneously lower z_{lwc} and raise z_{grd} in mixing zones.

Figure 5.6 also reveals another interesting feature: Lenschow *et al.* (2000) used cloud-top penetration flight legs to study the jump conditions across the cloud-top interface. They purposely flew at a nearly constant height to ensure that flights spent equal time inside and outside the cloud layer (as postulated by the horizontal straight line near 820 m shown in Fig. 5.6). By averaging data collected on either side of the cloud edge (with about 10 m segment on either side) from multiple cloud penetrations, Lenschow *et al.* (2000) constructed composite profiles of the mean temperature, moisture and ozone concentration, and used these profiles to infer the jump condition across the cloud-top interface. They found that these temperature and moisture jumps, though remaining sharp, are “considerably” smaller than those measured from ascending/descending sounding flights. Fig. 5.6 can help us understand this apparent discrepancy. Any cloud-top penetration flight leg along a horizontal straight line in the middle of the cloud-top undulations (as shown in Fig. 5.6) would miss most of the maximum $\partial\theta_l/\partial z$ areas and hence produce a considerably smaller mean Θ_l -jump across the interface than that measured from ascending/descending flight legs.

The fluctuating amplitude of the z_{grd} -interface is clearly much smaller than that of the z_{lwc} -interface, as evidenced from Fig. 5.6. The standard deviation of z_{lwc} is about 20 m computed from LES-1 and LES-3, and about 30 m from LES-2, all of which are commensurate with the observed value of 25m as derived from downward looking lidar during RF01. The standard deviation of z_{grd} is only about 7-8 m in all 3 LESs. The skewness of z_{lwc} ($\equiv \overline{z'_{lwc}{}^3} / \overline{z'_{lwc}{}^2}^{3/2}$) is about -2 and that of z_{grd} is around $-0.5 \sim -0.8$, in all LESs. (Note that in these calculations of standard deviation and skewness of z_{lwc} we exclude all “holes” where $z_{lwc} = 0$. If the holes are included, the liquid-water interface would yield a much larger negative skewness.) The large negative skewness of z_{lwc} is consistent with the highly intrusive (into the mixed layer) feature shown in Fig. 5.6.

5.3.2 Vertical profiles in the sharp-edged coordinate

One apparent advantage of the sharp-edged top coordinate is its ability to cleanly delineate the transition at the top of the boundary layer. However, even this can be ambiguous; as defined, z_{lwc} can delineate the cloud-top interface, but it may not adequately separate turbulent from non-turbulent air due to entrainment and evaporation at the cloud top. On the other hand, z_{grd} may better delineate the turbulence boundary, but not the cloud boundary as shown in Fig. 5.6.

Both interfaces, particularly z_{lwc} , are highly distorted which makes it difficult to average over using real data or LES flows. For instance, the interface is not guaranteed to remain single valued, and in the case of z_{lwc} it becomes undefined if no cloud exists in a column. For the LES cases studied here we do not experience multi-valued interfaces, and in regions where there is no cloud in a column, we interpolate z_{lwc} based on neighboring points for the purpose of constructing the z/z_{lwc} coordinate. This procedure is admittedly *ad hoc* but given nearly 100 % cloud cover in LES-1, it probably does not significantly bias our subsequent results.

Figure 5.7 compares the mean temperature, moisture and liquid water profiles averaged along the z/z_{lwc} coordinate with those averaged in the traditional smooth-top framework (i.e., z/\bar{z}_i) from LES-1. Note that z_{lwc} varies in x , y , and t , while \bar{z}_i varies only in t . The largest difference between the two averaging procedures shows up in the Q_l profile, which is expected given the definition of z_{lwc} . The changed coordinate, however, doesn't significantly affect the profiles of Θ_l and Q_T . The jumps of Θ_l and Q_T across the cloud top are not as sharp as one might have anticipated for a sharp-edged coordinate. (We do not plot the averages on the z/z_{grd} coordinate because they are essentially identical to the traditional smooth-top averages, mainly because the LES case analyzed here has a very sharp and strong capping inversion that is barely resolved even with our fine vertical grid spacing; the z_{grd} interface fluctuates within 1 to 2 vertical levels.)

It would be interesting to compare the flux profiles between the sharp-edged and smooth-top coordinates; as argued by Lilly (2002a,b) the minimum θ_l flux obtained from the smooth-top coordinate is much smaller than that obtained from the sharp-edged coordinate. However, we had trouble in constructing flux profiles for the sharp-edged coordinate from the LES solutions. Constructing the fluxes in such a coordinate requires computing the vertical velocity ω in the z/z_{lwc} coordinate (see Eq. 6.1 in Lilly 2002a), which involves taking the time and space derivatives of the highly distorted surface

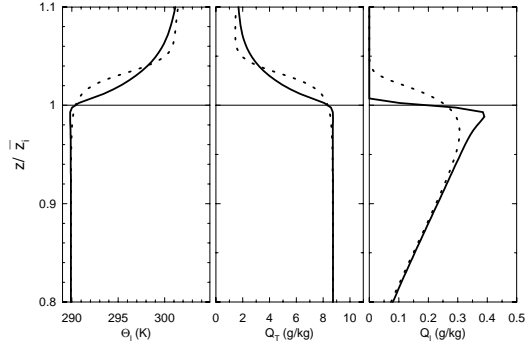


Figure 5.7. Profiles of Θ_l , Q_T and Q_l from LES-1 where solid curves represent averages along the z/z_{lwc} coordinate and dotted curves represent averages along horizontal planes. \bar{z}_i is the average of z_{lwc} .

z_{lwc} and hence is difficult to perform with either LESs or field measurements. In particular, ω becomes ill-defined near cloud-free columns where $z_{lwc} = 0$.

The difference between the entrainment θ_l -flux (denoted as $\overline{w\theta_{li}}$, and by definition is the flux averaged along the sharp-edged top) and the minimum θ_l -flux obtained from horizontal averaging was discussed by Lilly (2002a). Based on smoke-cloud LESs from Moeng et al (1999) and assuming a Gaussian distribution for smoke-top fluctuations, Lilly showed that the ratio of these two fluxes $\overline{w\theta_{li}}/\overline{w\theta_{l\min}} \sim e^{4s/\lambda}$, where s is the standard deviation of the interface fluctuations and λ is the decay length scale of longwave radiation as defined in section 5.1.1. From LES-1, $s \sim 20$ m using z_{lwc} as the interface and $\lambda \sim 26$ m, which yields $e^{4s/\lambda} \sim 20$. Figure 5.3 shows that $\rho_o c_p \overline{w\theta_{l\min}} \sim -38 \text{ Wm}^{-2}$, and since $\rho_o c_p \overline{w\theta_{li}} \equiv -\rho_o c_p w_e \Delta\Theta_l \sim -53 \text{ Wm}^{-2}$, their ratio is only about 1.4. Hence we conclude that Lilly's assumption of a Gaussian distribution for the interface fluctuations works only for smoke-cloud cases, not for wet-cloud cases.

5.4 Interface properties and stability

Lilly's second question is particularly relevant to RF01 and also well suited to evaluation by LES. He asks what characterizes the effective stability of the interface. This is essentially the same question which motivates the theoretical discussion presented in the chapter by Randall and Schubert in this volume. It arises because for stratocumulus, entrainment mixing occurs in conjunction with phase changes of water, and hence buoyancy of the mixtures doesn't depend linearly on mixing fraction. And because of the phase change of water, the entrainment buoyancy flux (i.e., the buoyancy flux along

the cloud-top interface where entrainment mixing occurs) does not simply equal $-w_e \Delta \Theta_v$.

5.4.1 Wetness of cloud-top interface

At the thin cloud-top interface, air is neither completely dry nor completely wet. To characterize the buoyancy flux at this thin interface, Lilly (2002b) defines a “wetness” factor α , which describes the moisture content of the interface, as

$$\overline{w\theta_{vi}} = \alpha \overline{w\theta_{vwi}} + (1 - \alpha) \overline{w\theta_{vdi}}, \quad (5.4)$$

where the dry (hypothetical) buoyancy flux is defined as

$$\overline{w\theta_{vdi}} = a_d \overline{w\theta_{li}} + b_d \overline{wq_{Ti}} \quad (5.5)$$

assuming the interface is completely dry, and the wet (hypothetical) buoyancy flux is defined as

$$\overline{w\theta_{vwi}} = a_w \overline{w\theta_{li}} + b_w \overline{wq_{Ti}} \quad (5.6)$$

assuming the interface is completely wet. The thermodynamic coefficients are $a_d = 1$ and $b_d \sim 175$ K for unsaturated air and $a_w \sim 0.54$ and $b_w \sim 1035$ K for saturated air, following Lilly’s thermodynamic approximation. Equation (5.4) makes the entrainment buoyancy flux depend strongly on the the wetness factor α . Rewriting (5.4) yields

$$\alpha = \frac{\overline{w\theta_{vdi}} - \overline{w\theta_{vi}}}{\overline{w\theta_{vdi}} - \overline{w\theta_{vwi}}}. \quad (5.7)$$

Lilly related this “wetness” factor to the mixing fraction of dry inversion air at which the mixture is just saturated, denoted as m_* . The concept of mixing fraction and how it modifies the buoyancy of mixtures has been used by many investigators (*e.g.*, Nicholls and Turton 1986, Kuo and Schubert 1988, Siems *et al.* 1990, Lilly 2002b) to explain interface instability. This instability factor has been explicitly incorporated into the entrainment rate parameterization of Turton and Nicholls (1987). The basic idea is explained with the help of Fig. 5.8, which was adapted from Fig. 3 in Stevens (2002).

The figure illustrates that the buoyancy of mixtures depends linearly on mixing fraction only when the mixtures are completely saturated ($m < m_*$) or completely unsaturated ($m > m_*$); these two linear curves have different slopes. The linear curve on the unsaturated side has a slope that satisfies

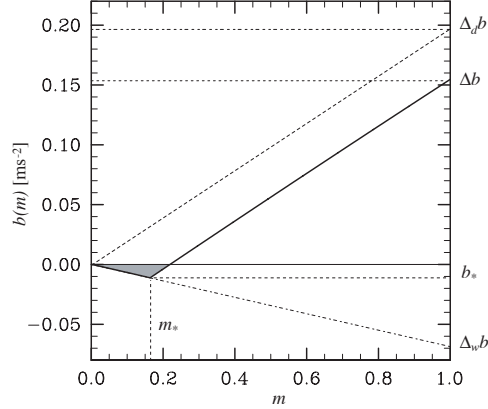


Figure 5.8. Buoyancy of mixtures of boundary layer air with a mass fraction, m , of above boundary layer air. Here the buoyancy, $b = g\delta\theta_v/\Theta_0$, measured relative to the boundary layer air, is plotted versus m . See text for further discussion.

the clear-air thermodynamic property:

$$\Delta_d\Theta_v \equiv a_d\Delta\Theta_l + b_d\Delta Q_T \quad (5.8)$$

while the linear curve on the saturated side has a slope that satisfies the cloudy-air thermodynamic property:

$$\Delta_w\Theta_v \equiv a_w\Delta\Theta_l + b_w\Delta Q_T. \quad (5.9)$$

The curves intersect at m_* where

$$m_* = \frac{\Delta_d\Theta_v - \Delta\Theta_v}{\Delta_d\Theta_v - \Delta_w\Theta_v}. \quad (5.10)$$

(A more detailed derivation of the above equation is given in Moeng *et al.*, 1995.)

There is a similarity between (5.7) and (5.10). Because $\overline{w\theta_{vdi}} = -w_e\Delta_d\Theta_v$ for completely unsaturated air and $\overline{w\theta_{vwi}} = -w_e\Delta_w\Theta_v$ for completely saturated air, Eqs. (5.7) and (5.10) imply that $\overline{w\theta_{vi}} = -w_e\Delta\Theta_v$ only if $\alpha = m_*$. Based on several LES solutions Lilly (2002b) argues that α is in general larger than m_* according to

$$\alpha = 1 - (1 - m_*)^{8/3}. \quad (5.11)$$

As discussed by Lilly, $\alpha = m_*$ only if no mixing occurs near the cloud top; for a typical stratocumulus where mixing does occur near the cloud top, $\alpha > m_*$.

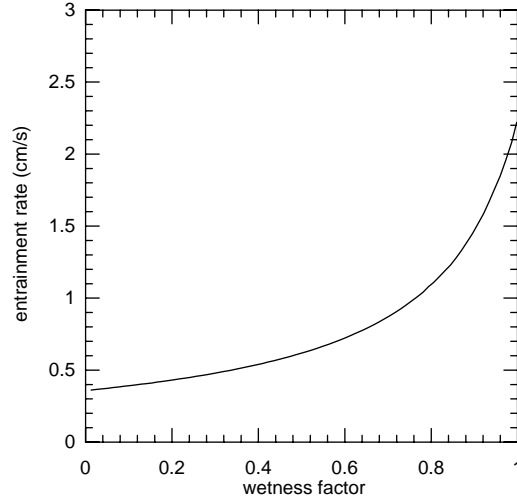


Figure 5.9. Dependence of the entrainment rate on the wetness factor, using Lilly’s new entrainment-rate formula (*i.e.*, equation (2.15) in Lilly, 2002b) and the LES-1 simulation fields.

LES-1 of RF01 allows us to check Lilly’s ideas using a case independent of those used by Lilly in calibrating the above relationships. From LES-1, we estimate $\Delta_w \Theta_v \sim -1.5$ K from (5.9) and $\Delta_d \Theta_v \sim 9.7$ K from (5.8) using Lilly’s values of a_d , a_w , b_d , and b_w . We also deduce the jump of mean virtual potential temperature from a mixing line analysis of θ_v and q_T (not shown), which produces $\Delta \Theta_v \sim 9$ K. Substituting these values into (5.10) yields $m_* \sim 0.06$ and in (5.11) gives $\alpha \sim 0.15$.

Alternatively α can be derived by picking the value that yields the best agreement between the entrainment rate obtained from Lilly’s new entrainment-rate formula [*i.e.*, equation (2.15) of Lilly (2002b)] and the simulated rate. We solve this graphically by plotting in Fig. 5.9 the dependence of the entrainment rate on the wetness factor α using the LES-1 results for surface fluxes, F_i , $\Delta_d \Theta_v$, $\Delta_w \Theta_v$, and the cloud-top-to-base ratio. Figure 5.9 shows a strong dependence of w_e on α , particularly when α becomes larger, *i.e.*, where the interface becomes wetter. (... Bjorn: Remember to update this figure!) For $w_e \sim 0.48$ cm s⁻¹ as in LES-1, Fig. 5.9 yields $\alpha \sim 0.3$. If we assume $\alpha = 1$ (a completely saturated interface), the entrainment rate would have been 4-5 times larger than this predicted value.

In the above, we have discussed the value of α based on a z_{lwc} interface where the layer below is completely wet and the layer above is completely dry. If the sharp-top interface is assumed to be z_{grd} , Fig. 5.6 suggests that

the interface would be close to completely dry because z_{grd} is mostly above z_{lwc} .

5.4.2 A new CTEI criterion

With his new entrainment-rate formula, Lilly (2002b) derived a new CTEI criterion, which can be summarized as

$$-\frac{L\Delta Q_T}{c_p\Delta\Theta_l} > F\left(\alpha, \frac{\bar{z}_b}{\bar{z}_i}\right), \quad (5.12)$$

where the right-hand side depends on the wetness factor and the ratio of the mean cloud-base (\bar{z}_b) to cloud-top heights. Lilly derived the above formula by setting the denominator of his entrainment-rate formula to zero such that the entrainment rate becomes infinitely large and hence corresponds to instability. We plot this new instability criterion as a function of α in Fig. 5.10 for three different \bar{z}_b/\bar{z}_i values; $\bar{z}_b/\bar{z}_i=0.77$ represents the DYCOMS-II RF01 case. In all cases this CTEI criterion is more stringent than the Deardorff-Randall criterion [which is 1.28 in terms of $-\frac{L\Delta Q_T}{c_p\Delta\Theta_l}$ and is the smallest value one can find in Fig. 5.10, where the cloud-top interface is assumed to be completely saturated (*i.e.*, $\alpha = 1$) and the cloud base zero]. The reasons Lilly's new criterion is more stringent are two fold: (i) the energetics of the whole layer, rather than just the cloud-top interfacial layer are considered in the entrainment formula; (ii) the buoyancy flux at the interface is a weighted combination of fluxes due to saturated and unsaturated mixtures rather than obtained by simply assuming all mixtures are saturated as has been done by Deardorff (1980) and Randall (1980).

For the DYCOMS RF01 case, $\bar{z}_b/\bar{z}_i \sim 0.77$ and $\alpha \sim 0.15 - 0.3$, and hence the jump ratio in (5.12) has to be larger than ~ 5 in order for instability (defined here as $w_e \rightarrow \infty$) to occur. The mixing line in Fig. 5.5 indicates that the jump ratio in the DYCOMS-II RF01 case is only about 1.6, which appears consistent with the sustenance of the cloud layer. Some other CTEI criteria (e.g., Kuo and Schubert 1988; Siems et al. 1990; MacVean and Mason 1990) might also predict a stable cloud layer for this RF01 case, but here we examine only Lilly's new criterion.

5.5 Summary

Large-eddy simulation provides scientists with an invaluable tool in their efforts to unravel the mysteries of flows beyond the reach of laboratories. The value of this tool depends in large part on the extent to which simulations

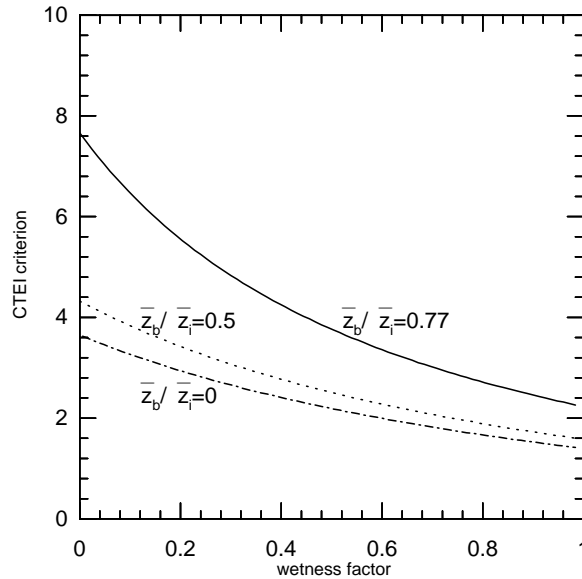


Figure 5.10. Dependence of the CTEI criterion on the wetness factor and the ratio of the cloud-base-to-top ratio calculated from equation (5.2) in Lilly (2002b).

are insensitive to the assumptions upon which they are based, for instance on the fidelity of the numerical representation of the resolved component of the flow, or the faithfulness with which the parameterized scales (both large and small) are represented. To illustrate these points we start with the construction of benchmark simulations, built around measurements derived from a recent field study. Comparisons between the simulations and the observed cloud evolution suggest that the simulations perform reasonably well. Moreover, sensitivity studies indicate that the LES representation is not markedly sensitive to the truncation of larger scales, and that details of the numerical representation only modestly affect the macroscopic statistics of the LES. The results of this benchmarking encourage the use of LES to investigate questions raised in two recent papers by Lilly (2002a,b).

The first question we address is motivated by Lilly's argument that the idealization of the stratocumulus topped boundary layer as a well mixed layer topped by a discontinuity in profiles of averaged state variables is most appropriate from the perspective of a coordinate system following the local cloud-top height. In contrast, the use of the geometrical height as the vertical coordinate artificially smoothes out the sharp jump over a layer equal to the depth of the cloud-top fluctuations. Because it resolves the three dimen-

sional structure of the cloud-top interface, LES is well suited to investigating questions relating to these possible choices of the vertical coordinate. It is shown that the conceptual simplicity of the interface-following coordinate is partially offset by ambiguity in defining the interface. In general, an interface defined by the cloud tops lies below the interface defined by the maximum gradient in temperature or moisture, and also fluctuates more. For this reason, the averaged statistics depend upon how one defines the interface. As a result we find it difficult to recommend one coordinate framework as clearly superior to the other.

The second question is what determines the effective stability of the cloud-top interface. With his new entrainment-rate formula, Lilly (2002b) derives a new criterion for the stability of the interface, and that criterion depends strongly on an interpolation factor (called wetness because it is related to the moisture content of mixtures) and the ratio of cloud-base to cloud-top heights. From the LES of the DYCOMS RF01 case, the wetness is estimated between 0.15 to 0.3 and the cloud-base-to-top ratio is about 0.77. These values yield a more stringent criterion compared to Deardorff-Randall's and put the RF01 cloud layer in the stable regime with respect to the interface stability.

References

- Betts, A.K. 1974: Reply to comment on the paper "Non-precipitating cumulus convection and its parameterization. *Quart J Roy. Meteor. Soc.*, **100**, 469–471.
- Deardorff, J.W. 1979: Prediction of convective mixed-layer entrainment for realistic capping inversion structure. *J. Atmos. Sci.*, **36**, 424–436.
- Deardorff, J. W., 1980: Cloud-top entrainment instability. *J. Atmos. Sci.*, **37**, 131-147.
- Koren, B., 1993: A robust upwind discretization method for advection, diffusion and source terms. In *Notes on Numerical Fluid Mechanics*, **45**, editors C.B. Vreugdenhil & B. Koren, pp. 117-138, Vieweg.
- Kuo, H., and W.H. Schubert 1988: Stability of cloud-topped boundary layers. *Quart. J. Roy. Meteor. Soc.*, **114**, 887–917.
- Lilly, D. K., 1968: Models of cloud-topped mixed layers under a strong inversion. *Quart. J. Roy. Meteorol. Soc.*, **94**, 292–309.
- Lilly, D. K., 2002a: Entrainment into mixed layers, Part I: Sharp-edged and smoothed tops. *J. Atmos. Sci.*, **59**, 3340-3352.

- Lilly, D. K., 2002b: Entrainment into mixed layers, Part II: A new closure. *J. Atmos. Sci.*, **59**, 3353-3361.
- MacVean, M.K., and P.J. Mason, 1990: Cloud-top entrainment instability through small-scale mixing and its parameterization in numerical models. *J. Atmos. Sci.*, **47**, 1012-1030.
- Moeng, C.-H., 1986: Large-eddy simulation of a stratus-topped boundary layer. Part I: Structure and budgets. *J. Atmos. Sci.*, **43**, 2886-2900.
- Moeng, C.-H., 2000: Entrainment rate, cloud fraction, and liquid water path of PBL stratocumulus clouds. *J. Atmos. Sci.*, **57**, 3627-3643.
- Moeng, C.-H., D.H. Lenschow, and D.A. Randall, 1995: Numerical investigations of the roles of radiative and evaporative feedbacks in stratocumulus entrainment and breakup. *J. Atmos. Sci.*, **52**, 2869-2883.
- Moeng, C.-H., P.P. Sullivan, and B. Stevens, 1999: Including radiative effects in an entrainment-rate formula for buoyancy-driven PBLs. *J. Atmos. Sci.*, **56**, 1031-1049.
- Nicholls, S., and D.J. Turton, 1986: An observational study of the structure of stratiform cloud sheets: Part II. Entrainment. *Quart. J. Roy. Meteorol. Soc.*, **112**, 461-480.
- Randall, D.A., 1980: Conditional instability of the first kind upside-down. *J. Atmos. Sci.*, **37**, 125-130.
- Siems, S.T., C.S. Bretherton, M.B. Baker, S.S. Shy, and R.E. Breidenthal, 1990: Buoyancy reversal and cloud-top entrainment instability. *Quart. J. Roy. Meteor. Soc.*, **116**, 705-739.
- Stevens, B., 2002: Entrainment in Stratocumulus Mixed Layers. *Quart. J. Roy. Meteor. Soc.*, **128**, 2663-2690.
- Stevens, B., C.-H. Moeng, and P. P. Sullivan, 1999: Large-eddy simulations of radiatively driven convection: sensitivities to the representation of small scales. *J. Atmos. Sci.*, **56**, 3963-3984.
- Stevens, B., Donald H. Lenschow, Gabor Vali, Hermann Gerber, A. Bandy, B. Blomquist, J.-L. Brenguier, C. S. Bretherton, F. Burnet, T. Campos, S. Chai, I. Faloon, D. Friesen, S. Haimov, K. Laursen, D. K. Lilly, S. M. Loehrer, Szymon P. Malinowski, B. Morely, M. D. Petters, D. C. Rogers, L. Russell, V. Savic-Jovicic, J. R. Snider, D. Straub, Marcin J. Szumowski, H. Takagi, D.C. Thornton, M. Tschudi, C. Twohy, M. Wetzell, and M. C. van Zanten, 2003a: Dynamics and Chemistry of Marine Stratocumulus. *Bull. Amer. Meteorol. Soc.*, **84**, 579-593.

- Stevens, B., D. H. Lenschow, I. Faloutsos, C.H. Moeng, D. K. Lilly, B. Blomquist, G. Vali, A. Bandy, T. Campos, H. Gerber, S. Haimov, B. Morley, D.C. Thornton, 2003b: On Entrainment Rates in Nocturnal Marine Stratocumulus. *Quart. J. Roy. Meteor. Soc.*, in press.
- Sullivan, P. P., C.-H. Moeng, B. Stevens, D. H. Lenschow, and S.D. Mayer, 1998: Structure of the entrainment zone in the convective atmospheric boundary layer. *J. Atmos. Sci.*, **55**, 3042–3064.
- Turton, J. D. and S. Nicholls, 1987: A study of the diurnal variation of stratocumulus using a multiple mixed layer model. *Quart. J. Roy. Meteor. Soc.*, **113**, 969–1009.